UNCLASSIFIED

AD 260 771

Reproduced
by the

ARMED SERVICES TECHNICAL INFORMATION AGENCY
ARLINGTON HALL STATION
ARLINGTON 12, VIRGINIA

UNCLASSIFIED

NOTICE: When government or other drawings, specifications or other data are used for any purpose other than in connection with a definitely related government procurement operation, the U. S. Government thereby incurs no responsibility, nor any obligation whatsoever; and the fact that the Government may have formulated, furnished, or in any way supplied the said drawings, specifications, or other data is not to be regarded by implication or otherwise as in any manner licensing the holder or any other person or corporation, or conveying any rights or permission to manufacture, use or sell any patented invention that may in any way be related thereto.

26027

RADC-TR-61-84

June 196

TECHNICAL REPORT

GUIDE TO THE STRUCTURAL DESIGN OF TRUNCATED SPHERICAL RIGID GROUND RADOMES

Robert B. Curtis

Rome Air Development Center
Air Force Systems Command
United States Air Force
Griffiss Air Force Base, New York

RADC-TR-61-84 June 1961

GUIDE TO THE STRUCTURAL DESIGN OF TRUNCATED SPHERICAL RIGID GROUND RADOMES

Robert B. Curtis

Project 5579
Task 45384

Rome Air Development Center
Air Force Systems Command
United States Air Force
Griffiss AFB, New York

AIR FORCE, Canterbury Press, Rome, N.Y., 8/2/61-227

FOREWORD

Acknowledgment is made to Dr. Eugene Sevin and Professor L.H. Donnell of Armour Research Foundation for their significant contributions to this study under contract AF 30(602)-1860 with Rome Air Development Center.

A B S T R A C T

A compilation of the analytical operations for the structural analysis of a truncated spherical shell based jointly upon an evaluation of research effort and operational performance is presented. The four primary problem areas of loading, shell conversion, stability, and strength which confront the engineer in the structural design of such a shell are discussed in detail. In each of these problem areas, computational methods or approaches are offered which may be adopted as design procedure.

P U B L I C A T I O N R E V I E W

This report has been reviewed and is approved.

Approved: J. J. Naresky

JOSEPH J. NARESKY
Chief, Applied Research Laboratory
Directorate of Engineering

Approved: for J. J. Naresky

WILLIAM F. BETHKE
Acting Director of Engineering
Directorate of Engineering

FOR THE COMMANDER: Irving J. Gabelman

IRVING J. GABELMAN
Director, Advanced Studies Office
DCS/Plans and Operations

TABLE OF CONTENTS

Contents	*Page*
INTRODUCTION	1
LOADING	1
SHELL CONVERSION	3
GENERAL STABILITY	4
LOCAL STABILITY	5
STRENGTHS	5
SUMMARY	7
RECOMMENDATIONS	7
REFERENCES	9
APPENDIX - A	10
APPENDIX - B	17
APPENDIX - C	23
APPENDIX - D	33

LIST OF ILLUSTRATIONS

Figures		*Page*
1.	Typical Radome Geometry	2
2.	Isobar Plotting on a 3/4 Spherical, Tower Mounted Radome (Ref. 2).	10
3.	Shell Coordinate System and Membrane Forces . .	11
4.	Comparison of Pressure Distribution . . .	15
5.	Comparison of Pressure Distribution (Polar Plot) .	15
6.	Geometry and Coordinates for Spherical Shell . .	24
7.	Determination of Semi-dimple Angle β . . .	26
8.	Load-Center Deflection Curves	29
9.	Meridional Stress Resultant N_ϕ	40
10.	Circumferential Stress Resultant N_θ . . .	40
11.	Shear Stress Resultant $N_{\phi\theta}$	41
12.	Stress Resultants on Circles X = constant . .	42
13.	Radial Displacement u	44
14.	Circumferential Displacement v	44
15.	Meridional Displacement w	45
16.	Deformed Shell in the Plane $\theta = 0°, 180°$ (u, w displacements)	45
17.	Deformed Shell in Base Circle Plane, $\phi = \phi_0 = 115°$ ($v = w = 0$, u displacements) . .	46
18.	Deformed Shell in Equatorial Plane, $\phi = 90°$ (u, v displacements)	46

GUIDE TO THE STRUCTURAL DESIGN OF TRUNCATED SPHERICAL RIGID GROUND RADOMES*

INTRODUCTION

The impetus for this report was generated by the Air Force's program in the development of truncated spherical rigid radomes for the environmental protection of ground radar and communication antennas. As such, this report should be of particular value to the engineer concerned with the structural analysis or design of these radomes; but the principles involved are equally applicable to any shell structure of the configuration mentioned. Although this report is primarily directed toward radome designers, no attempt will be made to discuss the electronic interaction of antenna and radome. Rather, it will be assumed that the radome or spherical shell design has progressed to the point where a tentative type of structure has been selected based upon transmission characteristics; and one must now determine by analysis what shell thickness, member sizes, skin thicknesses, and so forth, are required for structural adequacy under the imposed loading.

A significant portion of the material contained in this report was developed for Rome Air Development Center by Armour Research Foundation under contract AF 30(602)-1860. Appendixes A, C, and D of the final report[1] on this contract have been included in total in this report. This study program reflects the Air Force's belief that additional theoretical and experimental work was and still is required in this area. This belief was established from the kaleidoscope of analyses which have been submitted in response to operational requirements for radomes. This report represents an effort to establish common ground for contractor and Government engineers alike involved in the design of radomes.

In its capacity as responsible Center for the development of ground radomes, RADC has had the opportunity to gather data on all phases of the program from basic research to operational suitability. The procedures recommended herein are based jointly upon the evaluation of laboratory test data and appraisals of rigid radomes.

LOADING

Based upon observed field tests and reports from operational sites, it has been established that wind loading is of primary interest to the

*Released 14 February 1961.

structural engineer. Although snow and ice loadings represent a transmission hazard when one is considering a radome, experience has taught that for the typical geometry under consideration (Figure 1) there is not sufficient build-up of ice or snow to warrant serious structural consideration. Therefore this section of the report will discuss only the wind loading. Its analytical representation is presented in Appendix A.

Two types of analytical representations of wind load distribution on the spherical portion of the radome used in the past are

- potential flow distribution on a complete sphere, and
- distributions which approximate wind tunnel data on radomes of particular geometry.

The experimentally determined pressures agree well with potential theory on the forward half of the dome, but are substantially less than those predicted on the rear half. The differences are due principally to the fact that

- air does not act as an ideal fluid at the Reynolds numbers involved,
- turbulent flow occurs over the rear half of the dome,
- the presence of the base geometry (e.g., tower) cannot be ignored.

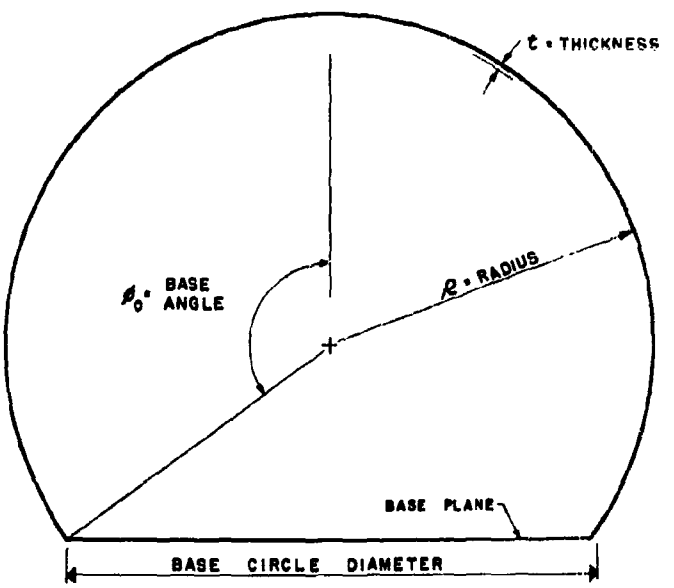

Figure 1. Typical Radome Geometry

The analytical representations, approximating the experimental data, imply a pressure distribution which is circularly symmetric with respect to the axis containing the stagnation point and in the direction of flow. The experimental results of Reference 2 on a 3/4 tower-mounted sphere (Figure 2, Appendix A) show this assumption of symmetry to be valid reasonably close to the stagnation point and also in the rear half of the dome, but in error on intermediate sections. However, a more complete analytical representation of the experimental data is impractical, especially from the viewpoint of subsequent analytical solution of the shell equations.

It is believed that, as a basis for stress analysis, a general polynomial representation of loading, providing that sufficient terms are retained, is preferable to the loading as predicted from potential theory on a complete sphere. The question, then, concerns the adequacy to which the particular series considered represents the available experimental data, say, in the vertical plane of symmetry of the dome. A three-term series preserves stagnation pressure and total lift and drag. As such, it closely approximates the experimental distribution near the stagnation point, but deviates markedly in the rear of the dome. The four-term series evaluated in Appendix A preserves, additionally, the location of the maximum suction pressure (see Figure 4, Appendix A). Of course, any desired degree of accuracy can be achieved by retaining sufficient terms in the series. Subsequent solution of the shell equations becomes more cumbersome, but remains feasible. Additional study is required to evaluate the practical significance of including terms beyond the fourth.

The situation is less involved with respect to stability considerations. Here it seems reasonable to base the dome design on the stagnation pressure assumed to act uniformly on the buckled area. Even if subsequent study indicates the nonuniformity of the pressure to be significant, the distribution according to potential theory, being valid for almost the entire forward half of the dome, should be adequate.

SHELL CONVERSION

In the theoretical work discussed in the following sections of this report, all formulas and computations will be based upon a structure with a uniform wall thickness of homogeneous, isotropic material. Unfortunately, the engineer rarely finds himself confronted with such an idealized structure. More often, the shell is a space frame with orthotropically oriented members or of sandwich construction with a wall of high density

high strength skins and low density, low strength core. To reduce these types of shells to a form which can be handled by a general analysis, they are converted to an equivalent homogeneous, isotropic, uniform thickness shell of such modulus of elasticity and thickness as to preserve the extensional and bending stiffness of the original structure. The elastically similar shell thus created will develop a loading and deflection pattern substantially identical to that of the original. The moments, shears, and thrusts computed on the basis of the equivalent shell are then considered as applied to the actual shell and existing stress levels computed.

Appendix B presents methods for the conversion of a sandwich structure and a space frame structure to their elastically equivalent uniform shells.

GENERAL STABILITY

Depending on construction, primary instability of a rigid radome shell can be caused

. by "oil canning" of the stagnation cap,

. by local buckling of the stiffeners in the case of space frames, or

. by local buckling of facings on one or more panels of sandwich construction.

To establish the general stability of the structure of interest, the designer must first convert the structure to its homogeneous, uniformly thick, elastically equivalent shell. This procedure is outlined in Appendix B. With the structural characteristics of the equivalent shell thus established, one may proceed to determine the critical buckling pressure or general stability of the structure.

As a part of this report, the general stability of a homogeneous spherical shell has been considered on the basis of energy techniques (Appendix C) from which the following has been indicated:

1. For design, it is reasonable to consider the stagnation pressure as being uniformly distributed over the buckled area.

2. For shells of the geometry considered (Figure 1), equation (37), Appendix C, predicts that the dimpled area will intersect the base circle for $\frac{r}{t} < 64$. This means that, for "thicker" shells, the base connections provide a stiffening effect not considered in theory.

3. The maximum stagnation or buckling pressure is given by equation (36), Appendix C, and the estimated size of dimple by equation (37),

Appendix C.

The mechanism of elastic buckling of complete spherical shells under uniform pressure is still somewhat of a mystery. The problem is compounded for a truncated sphere under nonuniform and especially nonaxisymmetric conditions, as is the case for radomes. Though lacking a fundamental understanding of the phenomena, it is believed that the present findings contribute to a rational basis for design. Continuing study should lead to further improvements of design procedures.

LOCAL STABILITY

Investigation of the local stability of an individual stiffener in a space frame proceeds along the lines of a conventional beam-column analysis. The axial load per stiffener is established from the normal loads per unit length of shell determined from the membrane analysis (Appendix D) multiplied by the effective spacing (Appendix B) of the stiffeners. This axial load, along with the transverse load transferred from the membrane, forms the combined loading picture on the stiffener. The degree of support or "end fixity" assigned to the stiffener is a direct function of the construction details peculiar to the structure of interest. Its evaluation depends upon the designer's experience and a thorough knowledge of these details, and does not lend itself to general treatment. With the loading and boundary conditions established, one may now proceed with any one of a number of familiar methods for the solution of indeterminate structures.

In the case of sandwich structures, once the general stability has been established, the local buckling of the faces on one or more panels may be determined by methods presented in Reference 3 of this report.

STRENGTHS

In general, stresses in radome shells have been determined employing curved column, simple beam, or membrane analyses, or combinations thereof. The curved column and beam analyses ignore the essential characteristics of a shell in that they disregard the influence of continuity and curvature on the geometrical relations between displacements and strains, and on the equilibrium conditions. Membrane theory, while incorporating these effects, takes no account of the flexural resistance of the shell and, as such, has definite limitations in its application. As will be discussed, these limitations, at the very least, make questionable estimates of the conditions of stress in the vicinity of the radome edge constraints.

What is required, then, is the application of a general bending theory to the problem of a truncated spherical shell. As of this writing, such a theory has not been developed; however, it is nonetheless feasible. A membrane solution, as discussed in Appendix D, may be viewed as a first step in obtaining the bending solution.

Membrane theory results from a simplification of the usual small deflection bending theory of elastic shells in which the moment resistance of the shell cross section is neglected. As a result, the state of stress at a point in the shell is completely specified in terms of two components of the resultant normal stress on the cross section and the resultant shear. Moreover, these stress resultants constitute a statically determinant system of forces, meaning that the governing (partial differential) equations can be solved, in principle, without regard to shell deformations. This has an important corollary, namely, that a membrane stress solution, in general, cannot be found which satisfies an arbitrarily specified system of boundary tractions or displacements.

With application to rigid radomes, this means that a membrane solution will not properly describe the built-in conditions at the base circle. Rather, the theory will predict a nonzero system of base displacements and associated curvatures. Since the actual edge conditions may be thought to result from the superposition of suitable edge shears and moments, it is clear that the membrane solution will be essentially meaningless insofar as base stresses are concerned.

One approach to the bending theory of shells involves a two-step solution. First, the membrane stresses are determined for the fully loaded shell and the deformations are computed at points of support. The second step involves evaluation of the bending theory for the shell subjected only to the necessary moments and shears at the points of support to remove the excess deformations predicted by the membrane solution. The complete solution is then the superposition of the stresses determined in the two preceding problems. Progress to date does not permit determination of the bending stresses. However, the membrane solution described in Appendix D was organized so as to readily permit the second step in the above procedure to be carried out at a later date. As indicated above, the results of the membrane solution are considered sufficiently accurate for design purposes at all points throughout the shell, except in the immediate vicinity of the base circle (that is, the boundary layer effect as Riessner terms it in Reference 4).

Since the designer more often finds himself involved with other than a uniform thickness shell of homogeneous material, the approach to a stress analysis must consider

. means of determining an "equivalent" homogeneous shell to represent the actual structure (Appendix B),

. the application of membrane theory (Appendix D) to determine the normal and shear loads in the equivalent shell, and

. the application of these loads to the actual shell and computation of the resulting stresses.

SUMMARY

In this report and the appendixes thereto, we have attempted to establish a norm or basis for a more rigorous analytical design of a radome or spherical shell. Beginning with the loading, a procedure for the analytical representation of the pressure distribution on a radome resulting from a wind loading has been indicated and worked out.

Secondly, methods for converting space frame structures and sandwich structures to their homogeneous, uniform wall thickness, elastic equivalent counterpart have been demonstrated. Once this has been accomplished, the designer may now apply the "membrane theory" to determine shell loads and investigate for general shell stability.

Third, a membrane analysis, which can be readily incorporated into a general bending theory, is presented which has been evaluated for a four term expansion of the loading and is considered valid in itself for that portion of the radome shell above the equatorial plane. The results of this analysis may now be applied to the actual structure under consideration, and local stability and strength requirements investigated.

Fourth, a new theory of the buckling of a complete spherical shell under uniform external pressure, developed by Professor L.H. Donnell of Armour Research Foundation, is presented as a part of this report. An approximate finite-displacement solution was obtained for the axisymmetric buckling, in the form of a single dimple of a fairly thin-walled homogeneous, elastic spherical shell. This solution provides for the buckling pressure, P_{cr}, and the semi-cone angle of the "dimple" which forms the buckled shape, β.

RECOMMENDATIONS

Based upon a general review of the design techniques, the following analytical studies are recommended:

. develop and evaluate in detail a general bending theory for uniform, homogeneous, spherical shells subject to the simplified wind loading of Appendix A, and incorporating the membrane analysis of Appendix D;

. extend the Donnell buckling theory presented in Appendix C to include more general characterization of the deflected shape;

. application of a more exact basis for determining the geometrical and mechanical properties of an "equivalent" homogeneous shell. One such theory due to E. Riessner (Reference 5) would appear to be particularly suited to radome structures.

REFERENCES

1. *Analytical and Experimental Studies of Spherical Rigid Ground Radomes*, Armour Research Foundation, Report ARF-8-154, Contract AF30(602)-1860, 1961.
2. RADC, Report No. UB-909-D-1, *Wind Tunnel Tests on a 1/24 Scale Model Air Supported Radome and Tower*, U.C., Cornell Aeronautical Laboratory, Inc., Sept 54.
3. ANC-23, *Sandwich Construction for Aircraft*, Part II, U.C., Forest Products Laboratory, Second Edition 1955.
4. "Membrane and Bending Stresses in Spherical Shells," U.C., *Journal of the Society for Industrial and Applied Mathematics*, Dec 56, Vol. 4, No. 4.
5. E. Riessner, NASA, No. 975.
6. Goodyear Aircraft Corporation No. 8224, *Theory of Spherical Ground Radomes*, May 1, 1958.
7. H.S. Tsien, "A Theory of the Buckling of Thin Shells," *Journal of the Aeronautical Sciences*, Vol. 9, No. 10, Aug 42.
8. L.H. Donnell, "Effects of Imperfections on Buckling of Thin Cylinders and Columns Under Axial Compression," *Journal of Applied Mechanics*, Mar 50.
9. T. Von Karman, and H.S. Tsien, "The Buckling of Spherical Shells by External Pressure," *Journal of Aeronautical Sciences*, Vol. 7, No. 2, Dec 39.
10. A. Kaplan and Y.C. Fung, *A Non-linear Theory of Bending and Buckling of Thin Elastic Shallow Spherical Shells*, National Advisory Committee for Aeronautics, TN 3212, Aug 54.
11. Timoshenko, *Theory of Plates and Shells*, McGraw-Hill Book Company, Inc., N.Y., 1940.
12. C.B. Biezeno and R. Grammel, "Elastic Problems of Simple Machine Elements," *Engineering Dynamics*, Vol. II, D. Van Nostrand Company, Inc., New York, 1954.

APPENDIX A

ANALYTICAL REPRESENTATION OF WIND LOADING

Typical data on steady wind pressures incident on radome shell geometries of the type considered (Figure 1) was obtained from Reference 2, and is summarized in Figure 2. With a view toward simplification, inspection of Figure 2 suggests replacing the given isobars by ones which are symmetrical with respect to the axis of flow (these isobars would appear as vertical lines in Figure 2). With this assumption, the wind pressure is a function only of the distance (measured in the direction of flow

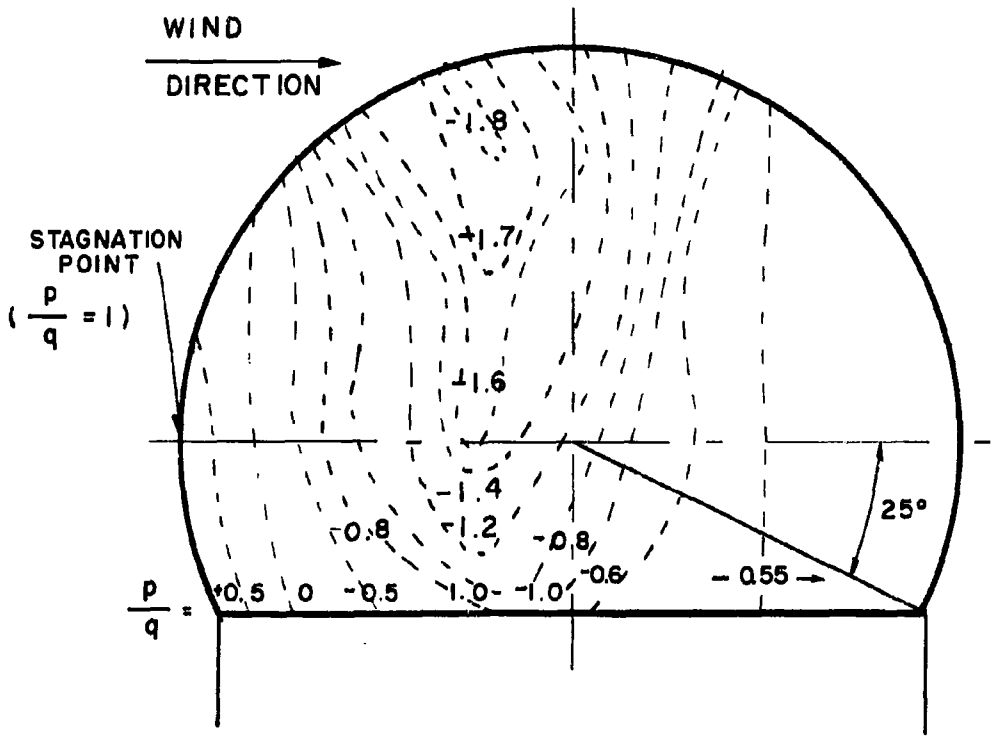

Figure 2. Isobar Plotting on a 3/4 Spherical, Tower Mounted Radome (Ref. 2)

from the stagnation point, x (see Figure 3).

For purposes of stress analysis, it is found convenient to express the normal pressure as a finite power series in the coordinate x, or, equivalently, in a cosine series in the meridian angle θ (Figure 3). The series form adopted is given in equation (1). Symbols are defined in the nomenclature.

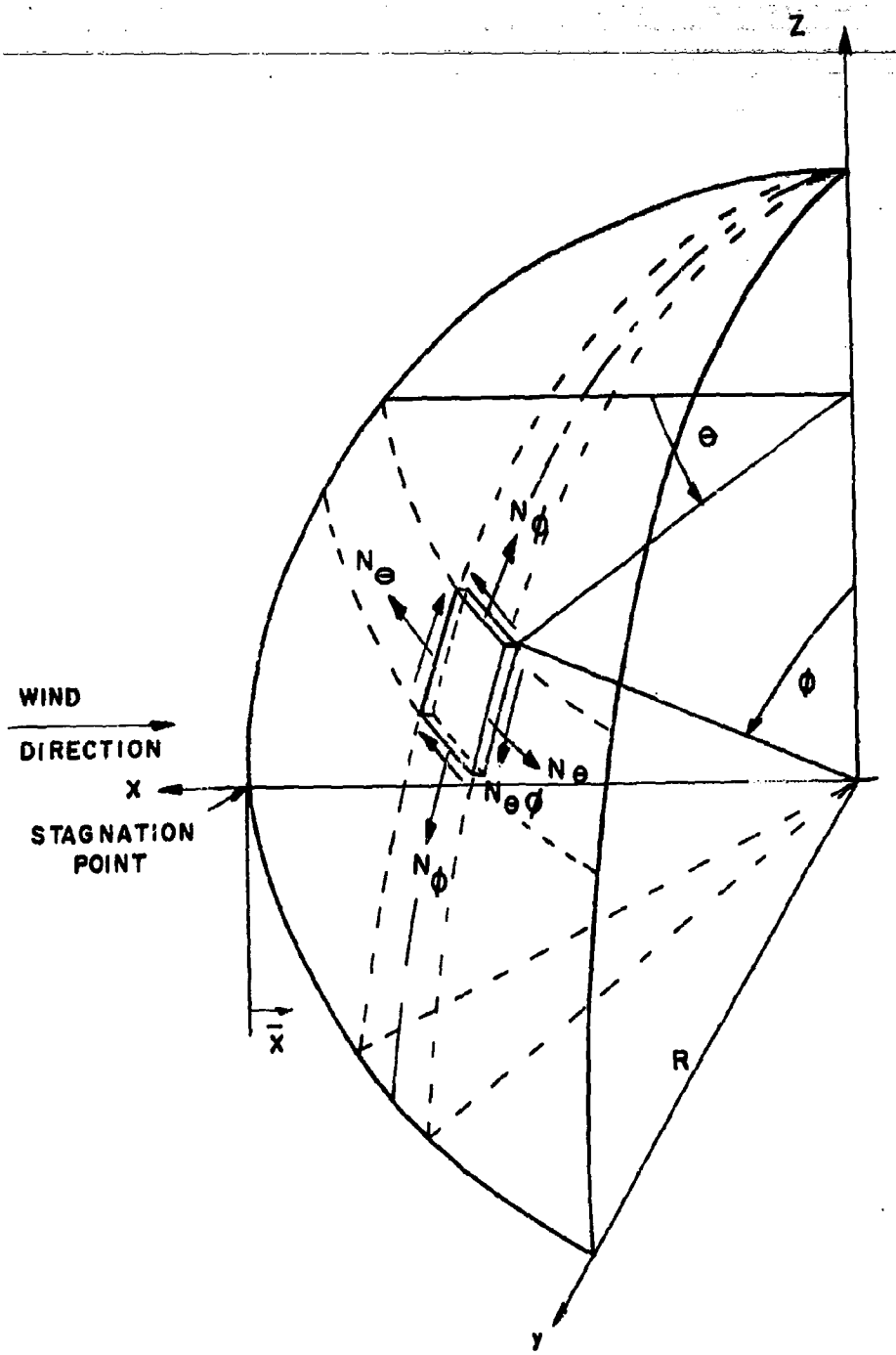

Figure 3. Shell Coordinate System and Membrane Forces

$$\frac{P_{(\phi,\theta)}}{q} = \sum_{n=0}^{N} a_n \overline{(x/R)}^n = \sum_{n=0}^{N} a_n (1 - \sin\phi \cos\theta)^n \qquad (1)$$

$$= \sum_{n=0}^{N} p_n(\phi) \cos n\theta,$$

where $a_0 = p_0(\phi) = 1$.

The coefficients $p_n(\phi)$ can be expressed in terms of the constants a_n by expanding equation (1) and equating coefficients in cos $n\theta$. The a_n, in turn, are related to those features of the actual pressure distribution which are to be retained. For $N = 3$, the following relations are obtained:*

$$\begin{aligned} p_0 &= A_0 + A_2 \sin^2\phi, \\ p_1 &= A_1 \sin\phi + 3A_3 \sin^3\phi, \\ p_2 &= A_2 \sin^2\phi, \\ p_3 &= A_3 \sin^3\phi, \end{aligned} \qquad (2)$$

where

$$\begin{aligned} A_0 &= a_0 + a_1 + a_2 + a_3, \\ A_1 &= -(a_1 + 2a_2 + 3a_3), \\ A_2 &= 1/2\ (a_2 + 3a_3), \\ A_3 &= -a_3/4. \end{aligned} \qquad (3)$$

The four coefficients $A_0 \ldots A_3$ are determined so as to preserve the total lift and drag on the radome (corresponding to the given pressure distribution), the stagnation pressure, and the position of the minimum average pressure. The first three conditions are clearly necessary, whereas the fourth condition is somewhat arbitrary. If more terms in equation (1) were retained, additional features of the given pressure distribution could be preserved.

In terms of the assumed pressure distribution, the total lift, L, and drag, D, on the radome shell are to be found to be:

* General relationships are derived but numerical results are presented only for $N = 3$.

$$L = -\int_{area} P_{(\phi\theta)} \cos\phi \, d\,\text{area},$$

$$\frac{L}{q} = -2R^2 \int_0^{\phi_0}\int_0^{\pi} \sum_{n=0}^{N} p_n(\phi) \cos\phi \sin\phi \cos n\theta \, d\theta \, d\phi \qquad (4)$$

$$= -2\pi R^2 \int_0^{\phi_0} p_0(\phi) \sin\phi \cos\phi \, d\phi,$$

$$D = \int_{area} P_{(\phi\theta)} \sin\phi \cos\theta \, d\,\text{area},$$

$$\frac{D}{q} = 2R^2 \int_0^{\phi_0}\int_0^{\pi} \sum_{n=0}^{N} p_n(\phi) \sin^2\phi \cos\theta \cos n\theta \, d\theta \, d\phi \qquad (5)$$

$$= \pi R^2 \int_0^{\phi_0} p_1(\phi) \sin^2\phi \, d\phi.$$

For $N = 3$, using equation (2)

$$\frac{L}{q} = -\frac{\pi R^2}{2} (2A_0 + A_2 \sin^2\phi_0) \sin^2\phi_0, \qquad (6)$$

$$\frac{D}{q} = \frac{\pi R^2}{15} [(5A_1 + 12A_3)(1 - \cos\phi_0)^2 (2 + \cos\phi_0) - 9A_3 \sin^4\phi_0 \cos\phi_0]. \qquad (7)$$

The condition for the pressure at the stagnation point, $\phi = \pi/2$, $\theta = 0$, is

$$\frac{p(\pi/2, 0)}{q} = 1 = \sum_{n=0}^{N} p_n(\pi/2).$$

For $N = 3$ this leads to

$$A_0 + A_1 + 2A_2 + 4A_3 = 1. \qquad (8)$$

If the position of the minimum pressure is prescribed, say, at $x = \sin\phi \cos\theta = x_m$, equation (1) yields

$$\left.\frac{d(P/q)}{dx}\right|_{x = x_m} = -\sum_{n=0}^{N} n a_n (1 - x_m)^{n-1} = 0. \qquad (9)$$

For $N = 3$, the a_n may be expressed in terms of the A_n by means of equation (3), and equation (9) becomes:

$$A_1 + 4A_2 x_m + 12 A_3 x_m^2 = 0.$$

The coefficients $A_1 \ldots A_3$ can now be determined from equations (6), (7), (8), and (9) once L/q, D/q, and x_π are specified.

Reference 2 reports the following experimentally determined values of total lift and drag for a 13.5 inch radius radome at a stagnation pressure of $q = 0.367$ psi (150 mph wind, one atmosphere wind tunnel pressure).

$L = 183$ lb,

$D = 52$ lb (extrapolated for full-scale Reynolds number).

Using these values, the following lift and drag coefficients were determined for a hemispherical radome ($\phi_0 = \pi/2$).

$$C_L = \frac{L}{\pi R^2 q} = \frac{183}{(0.367)(13.5)^2 \pi} = 0.87,$$

$$C_D = \frac{2D}{\pi R^2 q} = \frac{(2)(52)}{(0.367)(13.5)^2 \pi} = 0.50.$$

Reference 2 also indicates that the minimum average pressure in the plane $\theta = 0$ occurs at $x_\pi = \sin \phi_\pi = 0.2$ ($\phi_\pi = 11.5°$). Using the above values for C_L, C_D, and x_π, the A's are found to be,

$A_0 = -1.1433$

$A_1 = -0.6401$

$A_2 = 0.5466$

$A_3 = 0.4226$.

The numerical results of the stress analysis presented in Appendix D are based on these values. Figures 4 and 5 show a comparison of the average pressure data obtained from Reference 2 and the above power series expansion with $N = 3$.

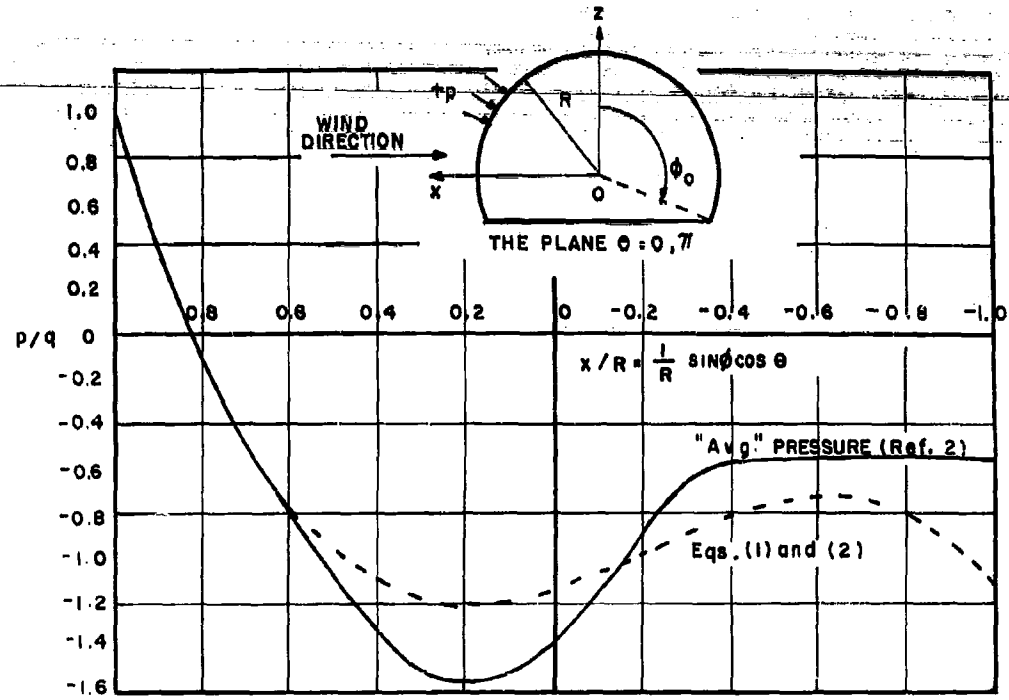

Figure 4. Comparison of Pressure Distribution

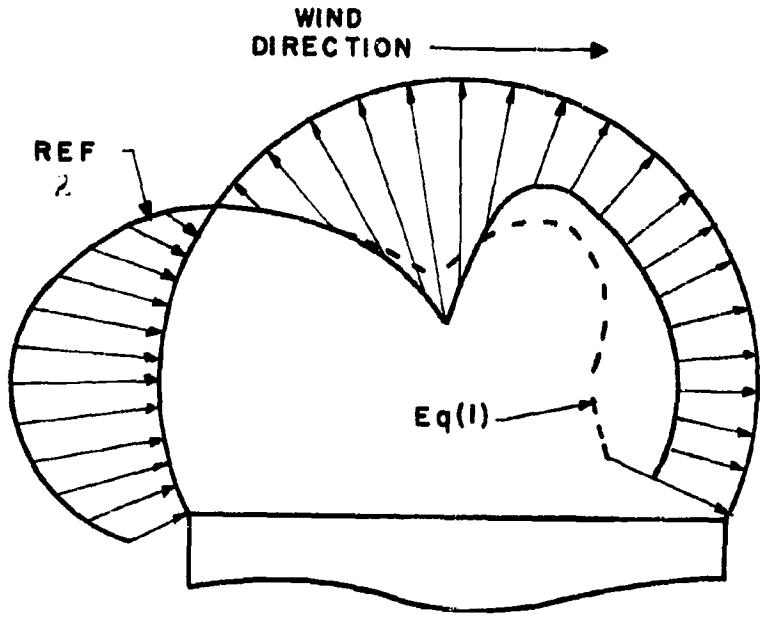

Figure 5. Comparison of Pressure Distribution (Polar Plot)

NOMENCLATURE FOR APPENDIX A

a_n, A_n	Load parameters,
C_D	Coefficient of drag,
C_L	Coefficient of lift,
D	Drag,
L	Lift,
q	Stagnation pressure,
P	Pressure normal to the undeformed shell surface,
p_n	Pressure distribution parameter,
$X, \bar{X}$	Shell coordinates (Figure 3),
R	Radius of shell,
θ	Meridional angle,
ϕ	Circumferential angle, and
ϕ_0	Angle of the base circle.

APPENDIX B

SHELL CONVERSION

The conversion of a sandwich or space frame type shell to its elastic equivalent often reflects the investigator's ingenuity and engineering judgment and, without a more exact solution, is difficult to evaluate. Thus, the choice of one method over another often is not unique but more a matter of opinion. The following methods have been used in the past and are recommended for continued use until such time as further study yields a more rigorous solution.

To create the elastically equivalent shell, the designer must preserve the extensional and bending stiffness of the actual structure. Representing extensional stiffness per unit width of structure as the product EA and the bending stiffness per unit width as the product EI, then the following relationships must be maintained between the actual and equivalent structures.

$$EI_{actual} = EI_{equivalent}$$

$$EA_{actual} = EA_{equivalent}$$

SANDWICH SHELL

In the case of the sandwich shell, the development continues as follows (Reference 3):

The general expression for the bending stiffness of a unit width of sandwich construction is:

$$EI_{actual} = \frac{E_F}{12\lambda_F}\left[t^3 - \rho t_c^3 - \frac{3\rho t_c \left(t_{F_1} - t_{F_2}\right)^2}{1 - \rho\frac{t_c}{t}}\right] \qquad (10)$$

where

$$\rho = 1 - \frac{E_c\,\lambda_F}{E_F\,\lambda_c} \text{ and } \left\{\begin{matrix}\lambda_F = 1 - \mu_F^2 \\ \lambda_c = 1 - \mu_c^2\end{matrix}\right\} .$$

This expression may be simplified by three postulations which are generally valid in the case of radome design:

1. Since the core is low density, low strength material, its stiffness may be neglected.

2. Skin thicknesses are equal (that is, $t_{F_1} = t_{F_2} = t_F$).

3. Since the skins are thin, their individual stiffnesses can be neglected.

Through application of these postulations, equation (10) may be reduced to:

$$EI_{actual} = \frac{E_F}{8\lambda_F} \; t_F(t + t_c)^2. \tag{11}$$

The bending stiffness of the equivalent shell per unit width is expressed as:

$$EI_{equivalent} = \frac{E_e \, t_e^3}{12 \, \lambda_F} \; . \tag{12}$$

Equating the actual and equivalent bending stiffness, equation (11) and (12) yield

$$E_e \, t_e^3 = \frac{3E_F \, t_F}{2} \; (t + t_c)^2. \tag{13}$$

Following the same procedure with extensional stiffness, the general expression for the extensional stiffness of a sandwich shell per unit width is:

$$EA_{actual} = E_F \; (t - t_c) + E_c \, t_c \; . \tag{14}$$

Again neglecting the modulus of elasticity of the core and assuming equal thickness skins, equation (14) becomes:

$$EA_{actual} = E_F \; (2t_F). \tag{15}$$

The extensional stiffness per unit width of the equivalent plate is expressed as:

$$EA_{equivalent} = E_e \, t_e \; . \tag{16}$$

Equating the extensional stiffness per unit width of the actual and equivalent shells, equations (15) and (16) yield:

$$E_e \, t_e = E_F(2t_F). \tag{17}$$

Solving equations (13) and (17) simultaneously yields the following expressions for the thickness and modulus of elasticity of the equivalent shell in terms of known parameters of the actual sandwich shell.

$$t_e = \frac{\sqrt{3}}{2} \quad (t + t_c),$$

$$E_e = \frac{\sqrt{4}}{3} \quad \frac{E_f t_f}{t + t_c}. \tag{18}$$

With the thickness and modulus of elasticity of the equivalent shell, one may now proceed to compute load distribution, deformation, and buckling pressure. However, it must be kept in mind that the actual stresses in the dome will be computed from the loads, determined from the equivalent shell per unit width, as applied to the actual shell of interest. In the case of the sandwich shell, the stresses in the core and facings due to these loads can be calculated by means of methods given in Reference 3.

SPACE FRAME

To develop the same equivalency for a space frame structure which resembles an irregular polyhedron, one must estimate the "effective spacing" served by each of the stiffeners comprising the irregular polyhedron. It has been demonstrated (Reference 6, p 95) that as the number of faces of a regular polyhedron increases, the stiffener stress under uniform pressure approaches the stress in a sphere of equivalent surface area similarly loaded whose thickness has been determined as follows:

$$t_s = \frac{\text{total vol of stiffeners}}{2 \text{ x surface area}}.$$

Only half the volume of the stiffeners has been equated to the volume of the shell because of the orthotropic nature of the stiffener as opposed to the isotropic nature of the shell. Since the stiffener stress and shell stress are now equal, one can say that the stiffener is now serving an effective length of shell (l_s) whose area is equal to that of the stiffener (A_s),

$$A_s = t_s \text{ x } l_s.$$

This length of shell will be used as the "effective spacing" of the stiffeners in developing the elastically equivalent shell as follows.

As in the case of the sandwich shell, the following equations must be satisfied:

$$EI_{actual} = EI_{equivalent} \quad \text{and}$$
$$EA_{actual} = EA_{equivalent}.$$

The bending stiffness per unit width of the stiffened shell is expressed as:

$$EI_{actual} = \frac{E_s I_s}{l_s}. \tag{19}$$

With the bending stiffness of the equivalent shell again expressed as in equation (12) and equating the two bending stiffnesses, we have:

$$\frac{E_s I_s}{l_s} = \frac{E_e t_e^3}{12 \lambda_s} \tag{20}$$

where

$$\lambda_s = 1 - \mu_s^2.$$

Proceeding in the same fashion with the extensional stiffness per unit width:

$$EA_{actual} = \frac{E_s A_s}{l_s}. \tag{21}$$

With the extensional stiffness of equivalent shell again expressed as in equation (16) and equating the two extensional stiffnesses, we have:

$$\frac{E_s A_s}{l_s} = E_e t_e. \tag{22}$$

Proceeding in a fashion identical to that with a sandwich and solving equation (20) and (22) simultaneously yields the following expressions for the thickness and modulus of elasticity of the equivalent shell in terms of known parameters of the stiffened shell,

$$t_e = 2\sqrt{\frac{3\lambda_s l_s}{A_s}}, \tag{23}$$

$$E_\theta = \frac{E_s A_s}{2 l_s}\sqrt{\frac{A_s}{3\lambda_s I_s}} \quad .$$

Once again the load distribution, deformations and buckling pressure may be computed based upon the elastically equivalent shell. To apply the load distribution, as determined from the membrane analysis (Appendix D) to the stiffened shell in terms of axial load per stiffener, one considers the stiffeners as assuming an axial load equal to the load carried by a length of the equivalent shell equal to the "equivalent spacing" developed for the stiffeners. This axial load, plus the transverse load resulting from the transfer of the wind load to the stiffener by the membrane, form the combined loading picture under which the stiffener is analyzed for local stability and strength.

NOMENCLATURE FOR APPENDIX B

EI_{actual}	Bending stiffness per unit length of actual shell under consideration
$EI_{equivalent}$	Bending stiffness per unit length of elastically equivalent shell
EA_{actual}	Extensional stiffness per unit length of actual shell under consideration
$EA_{equivalent}$	Extensional stiffness per unit length of elastically equivalent shell
E_F	Young's modulus of elasticity of sandwich skin material
E_c	Young's modulus of elasticity of sandwich core material
t	Over-all sandwich thickness
t_c	Core thickness
t_{F_1} t_{F_2}	Individual skin thickness when skins are unequal
t_F	Individual skin thickness when skins are equal
μ_F	Poisson's ratio of the skin
μ_c	Poisson's ratio of the core
E_e	Young's modulus of elasticity of elastically equivalent shell
t_e	Thickness of elastically equivalent shell
t_s	Thickness of equivalently stressed shell
A_s	Cross sectional stiffener area
l_s	"Effective spacing" of individual stiffeners in a grid work
E_s	Young's modulus of elasticity of stiffener material
I_s	Moment of inertia of stiffener cross section
μ_s	Poisson's ratio of stiffener material
λ	$(1 - \mu^2)$
ρ	$1 - \frac{E_c \lambda_F}{E_F \lambda_c}$

APPENDIX C

ENERGY THEORY OF SHELL BUCKLING (Reference 1)

Introduction

This Appendix presents an approximate solution, on the basis of energy techniques, for the buckling of a spherical shell under uniform external pressure. More specifically, a finite-displacement solution is obtained for the axisymmetric buckling, in the form of a single dimple, of a fairly thin-walled, homogeneous, elastic, spherical shell. The solution indicates that the pressure distribution outside of the dimple area is unimportant insofar as the buckling pressure is concerned. Hence, it appears that for buckling under wind pressures, the effective uniform pressure could be taken as the pressure at the stagnation point without great error. The theory provides explicit forms for the buckling pressure and the size of dimple in terms of the geometric and mechanical properties of the shell.

The present solution differs from previous studies of this type (e.g., Reference 7) in two principal respects:

- it takes into account a more general class of functions as characterizing the buckled shape; and
- it accounts for initial imperfections in the geometry of the shell.

The theory, of course, suffers none of the drawbacks of shallow shell theory especially in that no assumptions as to the boundary conditions at the edge of the dimple are introduced.

The following sections present the derivation of the governing equations, the method of solution, and the results obtained.

DERIVATION OF EQUATIONS

Figure 6 shows a section of a spherical shell of radius R and constant thickness t. The position of a point in the middle surface is located by means of the spherical coordinates, r,θ. The coordinate Z measures the distance of a point from the middle surface. The deformation of the middle surface is assumed to be radially symmetric, and is given in terms of a tangential displacement v and radial displacement ω, directed positive as shown in Figure 6. The middle surface is also assumed to have an initial radial deformation ω_i prior to application of the uniform normal pressure p.

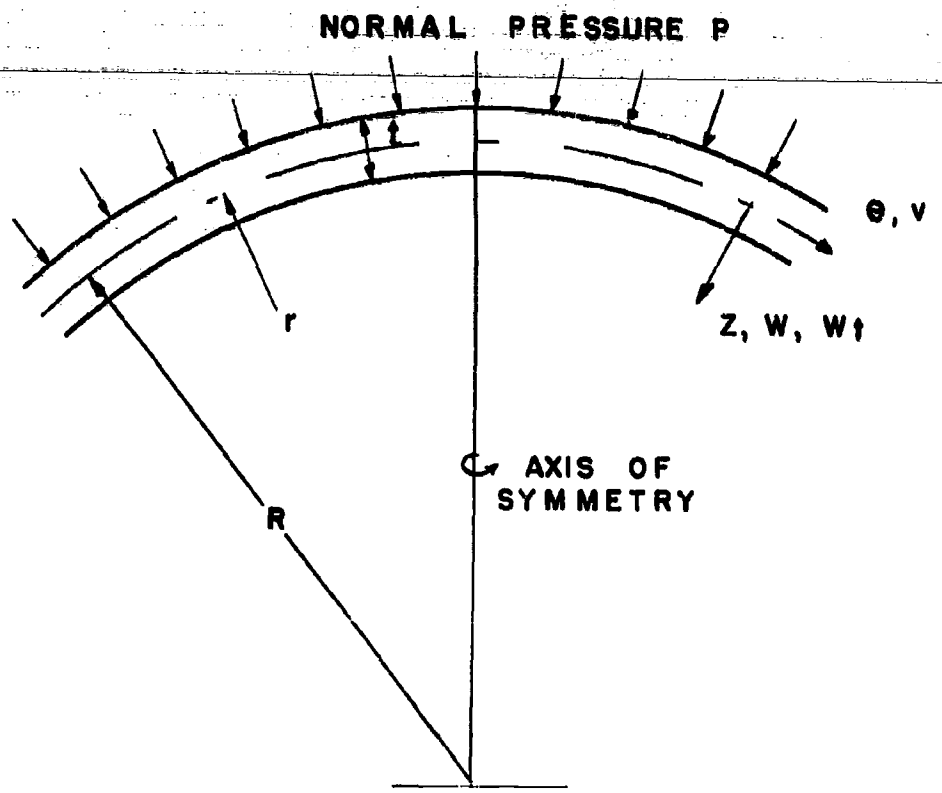

Figure 6. Geometry and Coordinates for Spherical Shell

From geometrical considerations the unit strains in the meridional direction, ϵ_m, and in the direction normal to this, ϵ_n, are

$$\epsilon_m = \frac{v}{r}\cot\theta - \frac{\omega}{r} - \frac{z}{r^2}\left(\frac{d\omega}{d\theta}\cot\theta + \omega\right)$$

$$\epsilon_n = \frac{1}{r}\frac{dv}{d\theta} - \frac{\omega}{r} + \frac{k}{2r^2}\left(\frac{d\omega}{d\theta}\right)^2 - \frac{z}{r^2}\left(\frac{d^2\omega}{d\theta^2} + \omega\right). \tag{24}$$

Following the methods of Reference 7, the parameter K is defined as

$$K = 1 + 2\frac{\omega_i}{\omega}, \tag{25}$$

and is assumed to be a constant. This means that only that component of

the initial radial deviation from spherical shape, ω_i, is considered which is the same shape as the deflection under load ω.

The total potential energy ϵ is

$$\epsilon = \frac{\pi r^2 E}{1-\nu^2} \int_{-t/2}^{t/2} \left(1 - \frac{z}{r}\right) dz \int_0^{\pi} (\epsilon_m^2 + \epsilon_n^2 + 2\nu\epsilon_m \epsilon_n) \sin\theta \, d\theta -$$

$$- 2\pi r^2 P \int_0^{\pi} \omega \sin\theta \, d\theta \qquad (26)$$

For simplicity in the derivation of equation (26), it has been assumed that the pressure p remains constant during displacement of the shell. It is believed that this will not introduce significant error if p is considered to be the average pressure during buckling.

The displacements ω and v are assumed to have the shape,

$$\omega = t e^{-\gamma^2} \sum_{m=1}^{\infty} W_m \gamma^m$$

$$m = 0, 2, 4 \ldots \text{even} \qquad (27)$$

$$v = \frac{t^2}{r} e^{-\gamma^2} \sum_{m=1}^{\infty} V_{m+1} \gamma_{m+1}$$

where

$$\gamma = \sqrt{\frac{rk}{t}} \, \theta. \qquad (28)$$

It is seen that the coefficient W_0 determines the amplitude of the dimple, and the other coefficients its precise shape. The number k determines the effective size of the dimple. A semi-angle of the dimple, β, may be defined somewhat arbitrarily in terms of k for given r/t. As shown in Figure 7, it seems reasonable to associate the value of $\gamma = 2.5$ with the angle β.

It will be observed that the expressions for displacement, equation (27), do not satisfy exactly continuity conditions on the opposite side of the sphere, $\theta = 180$ degrees. This is considered to be of no significance, however, since the displacements are completely negligible there.

METHOD OF SOLUTION

In the solution presented herein, only the coefficients W_0, V_1, and V_3

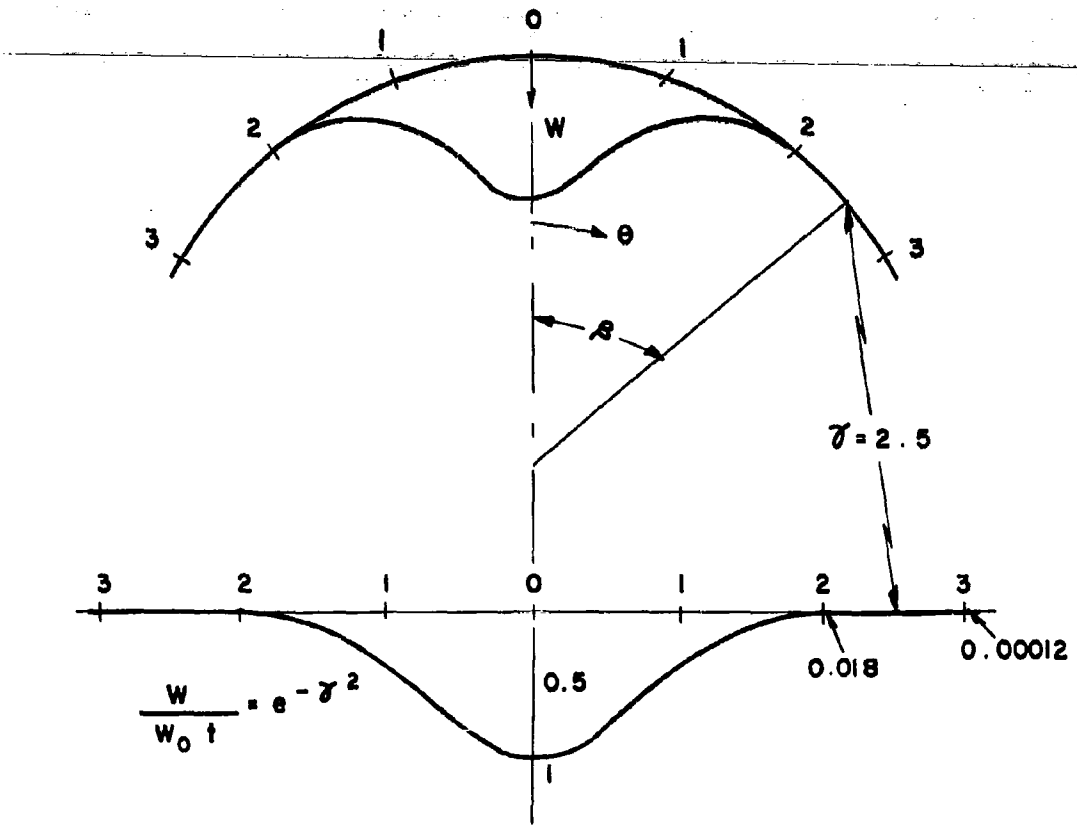

Figure 7. Determination of Semi-dimple Angle β

in equation (27) were considered, all other coefficients being taken zero. By means of equations (24), (26), and (27), and assuming the shell to be sufficiently thin so that $\frac{r}{t} k >> 1$ and $\frac{t}{r} k << 1$*, one finally obtains

$$\frac{3(1-\nu^2) r}{2\pi E t^4} \epsilon = \frac{3k}{4} (V_1^2 + V_1 V_3 + V_3^2) + W_0 \left(\frac{1}{k} + \frac{k}{4}\right) -$$

$$- W_0 (V_1 + V_3) + (2k W_0^2 + W_0 \Delta) \left[\frac{4}{27} V_3 - \right. \qquad (29)$$

$$\left. - \frac{2}{9k} W_0 + \frac{3}{128k} (2k W_0^2 + W_0 \Delta)\right] - \frac{3PW_0}{2k} ,$$

*The parameter k is of order unity.

where

$$P = \frac{(1 - \nu^2)\, P r^2}{E t^2}$$

$$\Delta = \frac{Ur}{t} . \tag{30}$$

Following Reference 8, the number U is considered to be an "unevenness factor," defined so that the initial radial deviation may be expressed as

$$\omega_i = a_1\, t\, e^{-\gamma^2}$$

and (31)

$$a_1 = \frac{U}{\pi^2}\, \frac{l^2}{t^2} = \frac{U r}{4Kt} = \frac{\Delta}{4k} .$$

Here, the term $l = \frac{\pi}{2}\sqrt{\frac{rt}{k}}$ is the approximate half wavelength of the radial displacement, taking the whole dimple as a full wave. This expression is similar to those used in studying the effects of imperfections in other buckling problems, see for example Reference 8. In these previous applications, it was argued that U should be roughly independent of the dimensions of the structure and should depend only on the manufacturing process. The factor U was found to be of the order of 0.0003, thus a value of $\Delta = \frac{Ur}{t} = 1$ corresponds to an extremely irregular shell unless r/t is very large.

Setting $\frac{\partial \epsilon}{\partial V_1} = \frac{\partial \epsilon}{\partial V_3} = 0$ in equation (29) according to the principle of virtual work, there results,

$$\frac{3k}{4}\,(2V_1 + V_3) - W_0 = 0,$$

$$\frac{3k}{4}\,(V_1 + 2V_3) - W_0 + \frac{4}{27}\,(2k W_0^2 + W_0\Delta) = 0. \tag{32}$$

Solving equation (32) for V_1 and V_3 we find

$$V_1 = \frac{4W_0}{9k}\left[1 + \frac{4}{27}(2k\,W_0 + \Delta)\right],$$

$$V_3 = \frac{4W_0}{9k}\left[1 - \frac{8}{27}(2k\,W_0 + \Delta)\right]. \qquad (33)$$

Now setting $\frac{\partial \epsilon}{\partial K} = \frac{\partial \epsilon}{\partial W_0} = 0$ in equation (29), and using equation (33) to eliminate V_1 and V_3, there finally results two equations relating P, and W_0 that is,

$$P = 0.37\,W_0\,(1 - 0.283\Delta + 0.024\Delta^2 - 0.45k^2) - 0.037k^2\,W_0^3, \qquad (34)$$

$$P = 0.74\,W_0\,(1 - 0.0283\Delta + 0.024\Delta^2 + 0.45k^2) - 0.625$$

$$(1 - 0.173\Delta)\,k\,W_0^2 + 0.146k^2\,W_0^3.$$

Eliminating P between these expressions, dividing by W_0, and simplifying, we obtain

$$(1.35 + 0.494\,W_0^2)\,k^2 - 1.69\,W_0\,(1 - 0.173\Delta)\,k + (1 - 0.283\Delta + 0.024\Delta^2) = 0. \qquad (35)$$

The desired relationship between P and W_0 (load-central deflection curve) can now be obtained by assuming values of Δ and W_0 solving equation (35) for k, and then solving either of equations (34) for P. The results of such calculations are shown in Figure 8 for the extreme values of the unevenness parameter $\Delta = 0$ and 1. It is observed that the load-deflection curves are not particularly dependent upon the value of Δ; the range $0 \leq \Delta \leq 1$ being extreme, with shells of practical interest in the vicinity of $\Delta = 0$. For this case, the value $P = 0.62$ may be taken as the nondimensional buckling load (Figure 8). From equation (30), the buckling pressure p_{cr} then has the value

$$p_{cr} = \frac{0.62Et^2}{(1 - \nu^2)r^2}. \qquad (36)$$

It is found that the values of k do not vary greatly, and average about 0.5 for the near horizontal parts of the curves in Figure 8. If, as previously mentioned in connection with Figure 7 the semi-angle of the dimple β is taken as $\gamma = 2.5$, then by equation (28) with $k = 0.5$,

$$2.5 = \sqrt{\frac{rk}{t}}\,\beta = \sqrt{\frac{r}{2t}}\,\beta,$$

or

$$\beta = 3.5\sqrt{\frac{t}{r}} \text{ (radians)}. \tag{37}$$

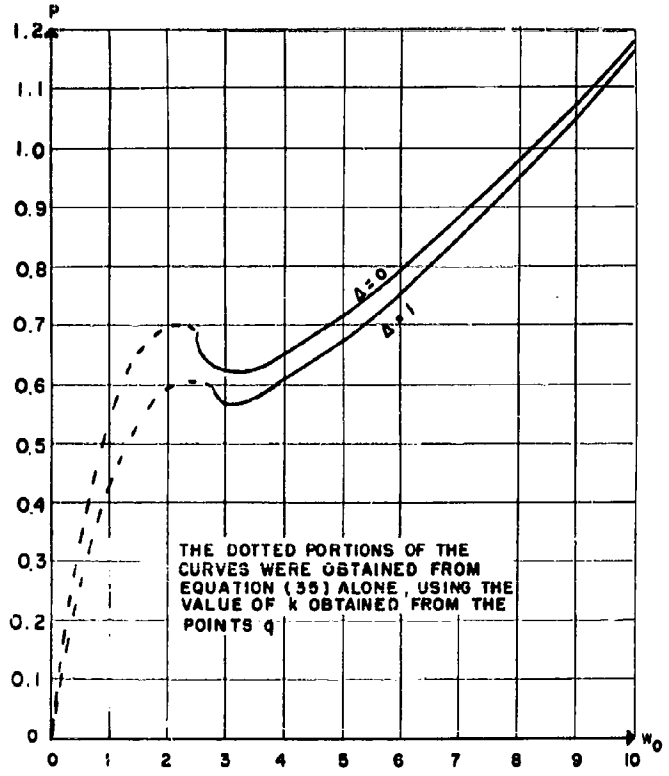

Figure 8. Load-center Deflection Curves

DISCUSSION OF RESULTS

The essential results of this study are contained in equations (36) and (37), namely, that the uniform pressure required to produce a dimple in the shell, p_{cr}, is about

$$p_{cr} = \frac{0.6Et^2}{(1-\nu^2)r^2},$$

and that the dimple formed has a semi-angle β (Figure 7) of about

$$\beta = 3.5\sqrt{\frac{t}{r}} \text{ radians} = 200\sqrt{\frac{t}{r}} \text{ degrees.}$$

The theory also points to a relatively small influence of geometric irregularities in the shape of the shell. Finally, equation (37) shows that for reasonably thin shells, the assumptions of shallow shell theory, aside from edge conditions, should be valid.

The general form of equation (36) can be considered to be well-established; the magnitude of the numerical coefficient 0.62, of course, is less well-established. In the one test result available in the literature for a full sphere, Reference 9, $E = 14.5 \times 10^6$ psi, $r/t = 900$ and the normal stress was $\frac{pr}{2t} = 2480$. These data correspond to a numerical coefficient of 0.31, just half the value given in equation (36). The material used is described as copper, so that yielding may have played some part in its failure. The value of β in this test is reported as eight degrees, while equation (37) gives 6.7 degrees for this case. However, the location of the "edge" of such a dimple is obviously rather indefinite.

In a recent series of unpublished tests at the Armour Research Foundation using ordinary ping pong balls, clear indication of the dimple formation was observed. Ping pong balls are found to be reasonably spherical shells for which $r/t = 50$ and $E = 5 \times 10^5$ psi and which collapse at about 100 psi. Using these data, the coefficient in equation (36) is determined to be 0.45 rather than 0.62. The angle β was measured as 30 degrees and predicted from equation (37) to be 28 degrees. Finally, the experimental data on clamped shallow shells reported in Reference 10 shows a coefficient of 0.4 in equation (36) to represent a lower bound on the collapse pressure; the value 0.62 falls in about the middle of the experimental data.

The present theory is approximate on several counts, chiefly in that the buckled shape is characterized by a minimum number of terms. The inclusion of additional terms would have the effect of reducing the numerical coefficient in equation (36). It is strongly recommended that work

on this theory be pursued. For the present, however, there is no basis for arbitrarily reducing this coefficient. It is believed therefore that equation (36) serves as a realistic basis for design with probably a minimum of conservation, and that the size of the dimple is given by equation (37).

In equations (37) and (38), E and t would be replaced by the expressions for E_e and t_e, as presented in Appendix B, to evaluate the critical buckling pressure for a space frame or sandwich design.

NOMENCLATURE FOR APPENDIX C

ϵ	total potential energy
k	dimple size parameter
$K = 1 + 2\,\omega_i/\omega$	constant, imperfection parameter
$l = \frac{\pi}{2}\sqrt{rt/k}$	wavelength of dimple
U	unevenness factor
v	circumferential displacement of shell
ω	radial displacement of shell
ω_i	initial radial deformation of shell
V_n, W_n	displacement parameter, equation (27)
z	radial coordinate
β	semi-angle of dimple
$\gamma = \sqrt{rk/t}\ \theta$	
$\Delta = Ur/t$	
r =	shell radius
ϵ_m	meridional strain
ϵ_n	circumferential strain
θ	circumferential angle
t	shell thickness
p_{cr}	critical buckling pressure
E	Young's modulus of elasticity of the material
ν	Poisson's ratio

$$P = \frac{(1-\nu^2)\ p_{cr}\ r^2}{Et^2}$$

APPENDIX D

In this section, a stress and deflection analysis of a homogeneous spherical radome shell of arbitrary base angle and subject to the wind pressure loading developed in Appendix A is carried out on the basis of membrane shell theory. It is intended that this analysis be considered as the first step in a two-step superposition approach to a general bending solution. The second step, not carried out, requires application of bending theory to a radome subject only to edge tractions sufficient to compensate for edge deflections and rotations implied in the membrane solution. Toward this end, the membrane solution is adjusted to yield only radial deflections at the edge. This solution is considered valid for that portion of the radome shell above the equatorial plane. These results, especially with regard to deflections, are believed to be more complete than heretofore available.

MEMBRANE ANALYSIS

Stresses - Figure 3 shows the membrane forces which act on an element cut from a spherical shell by two adjacent meridians and two parallel circles. The notation and sign convention for the stress resultants conform to that of Reference 11. The equations of equilibrium of the element are summarized in equation (38) and serve to determine the resultant meridional force N_ϕ, the circumferential force N_θ, and the shearing forces $N_{\theta\phi} = N_{\phi\theta}$. All of the forces (that is, stress resultants) are per unit length of the shell section.

$$\frac{\partial}{\partial\phi}(N_\phi \sin\phi) + \frac{\partial N_{\theta\phi}}{\partial\theta} - N_\theta \cos\phi = 0;$$

$$\frac{\partial}{\partial\phi}(N_{\phi\theta} \sin\phi) + \frac{\partial N_\theta}{\partial\theta} + N_{\theta\phi} \cos\phi = 0, \qquad (38)$$

$$[N_\phi + N_\theta + P_{(\phi\theta)}R] \sin\phi = 0,$$

where $P_{(\phi,\theta)}$ is the pressure distribution normal to the undeformed shell surface. A solution to equation (38) is sought which leads to finite stresses at the shell apex, $\phi = 0$. The condition that the resultants of the edge tractions on the base circle ϕ_0 are in equilibrium with the resultants of the applied forces than is automatically satisfied.

Using the pressure distribution $P_{(\phi,\theta)}$ described in the previous

section, equation (1), and following Reference 10, a solution of equation (38) is assumed in the form

$$N_\phi = Rq \sum_{n=0}^{N} S_{\phi n}(\phi) \cos n\theta,$$

$$N_\theta = -N_\phi - RP_{(\phi,\theta)}, \tag{39}$$

and

$$N_{\phi\theta} = Rq \sum_{n=0}^{N} S_{\phi\theta n}(\phi) \sin n\theta.$$

Equation (38) is then reduced to a pair of ordinary differential equations in $S_{\phi n}$ and $S_{\phi\theta n}$ which can be integrated to yield

$$\begin{aligned} S_{\phi n} &= \tfrac{1}{2}(U_n + V_n) \\ S_{\phi\theta n} &= \tfrac{1}{2}(U_n - V_n). \end{aligned} \tag{40}$$

Where, letting

$$C = \cos\phi,$$

$$S = \sin\phi,$$

$$\begin{aligned} U_n &= -(1+C)^{n/2} S^{-n-2} [I_{1n}(\phi) - I_{1n}(0)], \\ V_n &= (1-C)^{n/2} S^{-n-2} [I_{2n}(\phi) - K_n], \end{aligned} \tag{41}$$

and

$$\begin{aligned} I_{1n}(\phi) &\int p_n(\phi)(n+C)(1-C)^n S^{1-n} d\phi, \\ I_{2n}(\phi) &\int p_n(\phi)(n-C)(1+C)^n S^{1-n} d\phi, \end{aligned} \tag{42}$$

$$K_n = \begin{cases} I_{2n}(0) & \text{for } n = 0,1 \\ \text{arbitrary for } n \geq 2. \end{cases}$$

The integral expressions, equation (42), can be evaluated once the pressure coefficients $P_n(\phi)$ are specified. As seen from equation (2), these will generally be of the form

$$P_n(\phi) = \sum_{j=0}^{J} A_{n+2j} (\sin\phi)^{n+2j}; \quad J \leq N.$$

While it is possible to evaluate equation (42) for the j^{th} general term, there is little advantage in doing so for small N. Explicit results for

$N = 3$ are given below for the $P_n(\phi)$ defined in equation (2).

$$S_{\phi 0} = -\frac{A_0}{2} - \frac{A_2}{4} S^2$$

$$S_{\phi 1} = -C(1-C)^2 S^{-3} \left[\frac{A_1}{3}(2+C) + \frac{A_3}{5}(1-C)(3C^2+9C+8)\right]$$

$$S_{\phi 2} = -\frac{A_2}{4}(2+S^2) + K_2 (1+C)^{-2}$$

$$S_{\phi 3} = -\frac{A_3}{5}(3+S^2) S + K_3 S(1+C)^{-3}$$

$$S_{\phi\theta_0} = 0$$

$$S_{\phi\theta_1} = S_{\phi_1} C^{-1}$$

$$S_{\phi\theta_2} = \frac{A_2 C}{2} - K_2 (1+C)^{-2}$$

$$S_{\phi\theta_3} = \frac{3}{5} A_3 SC - K_3 (1+C)^{-3},$$

where, as before, $C = \cos\phi$, $S = \sin\phi$.

We observe from equation (43) or equation (42), that the stress functions for $n \geq 2$ are not uniquely defined. This results from the fact that the pressure terms for $n \geq 2$, equation (1), produce no resultant force or moment on the shell, and it would be necessary to specify a compatible distribution of stress on the base circle in order to establish a unique membrane solution. In the present case, of course, only displacement conditions are known at the base circle, and nothing is known concerning the stresses. Thus, the membrane solution determined is unique only to within an arbitrary system of self-equilibrated stresses applied to the base circle. The way out is to consider this solution as the first step in a two-step procedure leading to the determination of the bending stresses as described in the section on Strengths. The constants of integration, K_n, appearing in equation (43) can then be arbitrarily determined and the resulting deformations accounted for in the second step of the solution. If one considers the shell to be fully restrained against displacements at

the base circle, the K_n are most conveniently chosen by requiring two of the three components of the base displacements to be zero, thus leaving only one displacement to be eliminated by base moments and shears. This evaluation is presented in the following section.

SHELL DISPLACEMENTS

Following Reference 12, the displacement components u, v, w (measured, respectively, in the positive radial, circumferential (θ), and meridional (ϕ) directions) can be related to the stress resultants by means of the following system of partial differential equations.

$$\frac{\partial v}{\partial \theta} - W \cos \phi + \frac{\partial w}{\partial \phi} \sin \phi = \beta \, (N_\theta - N_\phi) \sin \phi,$$

$$\frac{\partial w}{\partial \theta} + V \cos \phi - \frac{\partial v}{\partial \phi} \sin \phi = -2\beta \, N_{\theta\phi} \sin \phi, \qquad (44)$$

$$u = \frac{\beta}{1+\nu} (N_\phi - \nu N_\theta) + \frac{\partial w}{\partial \phi} ,$$

where,

$$\beta = \frac{R(1+\nu)}{Et} .$$

This system of equations can be integrated in a fashion similar to that employed for equation (38). Thus, we assume a solution in the form

$$u = \sum_{n=0}^{N} u_n(\phi) \cos n\theta,$$

$$v = \sum_{n=0}^{N} v_n(\phi) \sin n\theta, \qquad (45)$$

$$w = \sum_{n=0}^{N} w_n(\phi) \cos n\theta.$$

Using equations (39) and (45) and after considerable manipulation, the following solutions to equation (44) are obtained:

$$v_n = -\tfrac{1}{2}\beta RS^{1-n}\left[(1+C)^n (J_{1n}\phi - L_n) - (1-C)^n (J_{2n}(\phi) - M_n)\right],$$

$$w_n = -\tfrac{1}{2}\beta RS^{1-n}\left[(1+C)^n (J_{1n}\phi - L_n) + (1-C)^n (J_{2n}(\phi) - M_n)\right], \tag{46}$$

$$u_n = S^{-1}(Cw_n - nV_n) - \frac{\beta R}{1+\nu}\left[(1+\nu)\, S_{\phi n} + p_n\right]$$

where,

$$J_{1n}(\phi) = \int (2S_{\phi n} - 2S_{\phi\theta n} + p_n)(1-C)^{n_S - n - 1}\, d_\phi\ ,$$

$$J_{2n}(\phi) = \int (2S_{\phi n} + 2S_{\phi\theta n} + p_n)(1+C)^{n_S - n - 1}\, d_\phi\ .$$

$$L_n = \begin{cases} \text{arbitrary} & \text{for } n = 0,1 \\ J_{1n}(0) & \text{for } n \geq 2 \end{cases} \tag{47}$$

$$M_n = \text{arbitrary} \quad \text{for } n \geq 0,$$

and where $S_{\phi n}$ and $S_{\phi\theta n}$ are given by equations (40), (41) and (42) and p_n is determined from equation (1).

The following results are obtained for J_{1n} and J_{2n} for $N = 3$.

$$J_{10}(\phi) = J_{20}(\phi) = -\frac{A_2 C}{2}\ ,$$

$$J_{11}(\phi) = \frac{A_1}{3}(2m^{-2} + 2m^{-1} - lnm) + \frac{A_3}{10}(16m^{-2} + 16m^{-1} + 9m^2 - 24m - 8\,lnm + 45),$$

$$J_{21}(\phi) = \frac{A_1}{3}lnm + \frac{A_3}{10}(-9m^2 + 12m + 8lnm + 15),$$

$$J_{12}(\phi) = \frac{4}{3}K_2 m^{-3} + \frac{A_2 C}{2}\ , \tag{48}$$

$$J_{13}(\phi) = \frac{2}{3}K_3 (1-2C)\, m^{-4} - 3\frac{A_3}{10}(1-C)^2,$$

$$J_{23}(\phi) = \frac{3}{10}A_3 m^2,$$

$$J_{22}(\phi) = \frac{A_2 C}{2}\ ,$$

where,

$$m = 1 + C = 1 + \cos \phi.$$

EVALUATION OF INTEGRATION CONSTANTS

It is observed from the results of the preceding two sections that for terms up to $n = N$ (actually $N + 1$ terms since $n = 0$ is counted), there is a total of $2N + 2$ integration constants consisting of $N - 1$ constants in the stress equation, equation (40), and $N + 3$ constants in the displacement equation, (45). Since there are $3N + 3$ components of displacement to be specified at the base circle, it is evident that the membrane theory cannot possibly serve as a complete solution to the problem. This, of course, was stated at the outset. It is proposed to evaluate these constants by setting the $2N + 2$ components of the v and w displacements equal to zero at the base circle, $\phi = \phi_0$. This will provide a solution for a shell having only radial displacements, $u(\phi_0) = u_0$, at the base circle. The complete solution for the fully restrained shell then can be obtained by solving the general bending equations for a system of edge moments and shears which remove the u_0 displacements, as mentioned previously.

The $2N + 2$ equations for the integration constants are obtained by setting $v_n(\phi_0) = w_n(\phi_0) = 0$ in equation (46). There results

$$\begin{aligned} L_n &= J_{1n}(\phi_0) && \text{for } n = 0,1 \\ J_{1n}(\phi_0) &= J_{1n}(0) && \text{for } n \geq 2, \\ M_n &= J_{2n}(\phi_0) && \text{for } n \geq 0, \end{aligned} \tag{49}$$

where the J_{1n} contain the $N - 1$ unknown constants, $K_n (N \geq 2)$. Since $v_n = w_n = 0$ on $\phi = \phi_0$, the components of radial displacement at the base circle are, from equation (46),

$$u_n(\phi_0) = u_{0n} = \frac{\beta R}{1 + \nu} \left[(1 + \nu) \, S_{\phi n}(\phi_0) + p_n(\phi_0) \right]. \tag{50}$$

For $N = 3$, the eight integration constants are K_2, K_3, L_0, L_1, M_0, M_1, M_2, and M_3. Letting $m_0 = 1 + \cos \phi_0$, these are found to be,

$$K_2 = \frac{3A_3\,(2 - m_0)}{8\,m_0^{-3} - 1},$$

$$K_3 = \frac{36A_3\,(2 - m_0)^2}{80\,(3 - 2m_0)^{-4} + 5},$$

$$L_0 = N_0 = -K_2 = \frac{A_2}{2}\,(1 - m_0), \tag{51}$$

$$L_1 = \frac{A_1}{3}\,(2m_0^{-2} + 2m_0^{-1} - \ln m_0) + \frac{A_3}{10}\,(16\,m_0^{-2} +$$

$$+ 16m_0^{-1} + 9m_0^{2} - 24\,m_0 - 8\,\ln m_0 + 45),$$

$$N_1 = \frac{A_1}{3}\,\ln m_0 + \frac{A_3}{10}\,(-9\,m_0^{2} + 12\,m_0 + 8\,\ln m_0 + 15),$$

$$N_3 = \frac{3}{10}\,A_3\,m_0^{2}.$$

Using these values, the stress resultants and displacements at any point (ϕ, θ) in the shell can be found by means of equations (2), (11), (39), (43), (45), (46), (48), (50) and (51).

NUMERICAL RESULTS

The stress resultants and displacements for $N = 3$ were programed for computation on an IBM-650 digital computer. Input to the program consists of the base circle angle ϕ_0, Poisson's ratio ν, the load parameters A_0, A_1, A_2, and A_3, and information as to the number and location of points in the shell at which stresses and displacements are to be determined. Output consists of total and component stresses, deflections, and load at each point. These values are based on unit stagnation pressure, σ, and unit shell parameter Et/R^2. Actual stresses and deflections for a specific load and shell are obtained by a simple multiplication.

Typical results for $\phi_0 = 115°$, $\nu = 0.25$, and $A_0 \ldots A_3$ as given in Equation (48) are shown in Figures 9 through 18. Figures 9, 10, and 11 show the distribution of the stress resultants on a series of parallel circles, ϕ = constant.

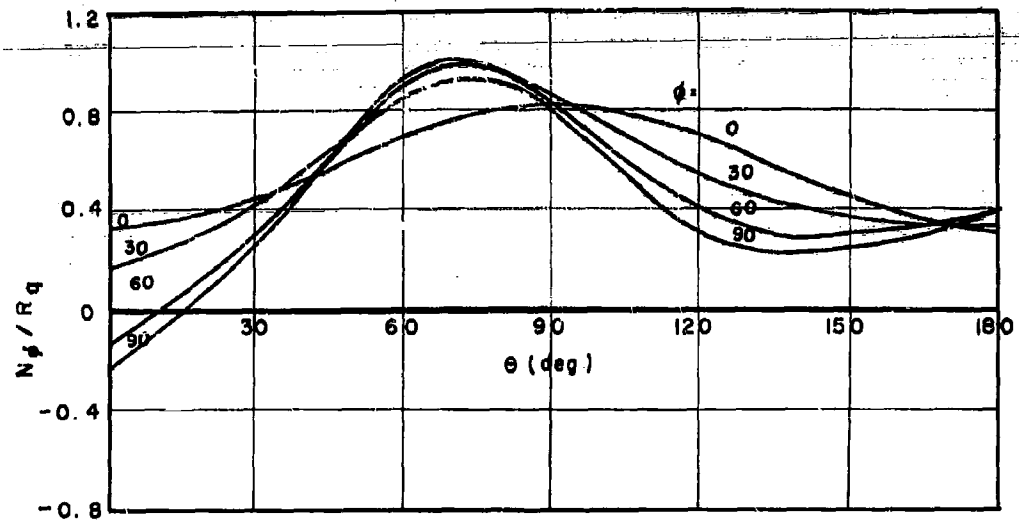

Figure 9. Meridional Stress Resultant N_ϕ

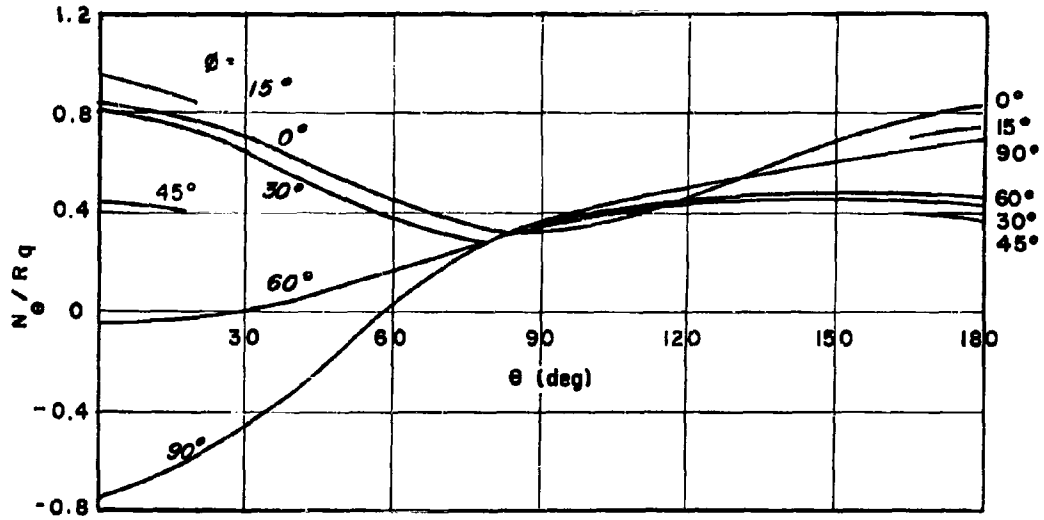

Figure 10. Circumferential Stress Resultant N_θ

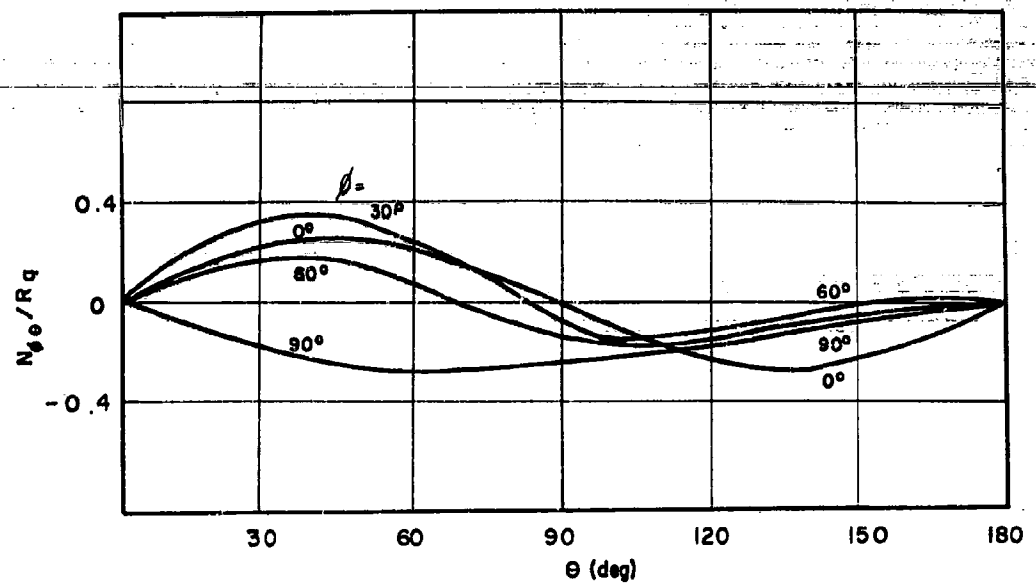

Figure 11. Shear Stress Resultant $N\phi\theta$

Inasmuch as the membrane stresses are not an adequate representative of total stresses in the vicinity of the base circle, results are shown only for points on the shell lying on or above the equatorial plane, that is, for $\phi \geq 90$ degrees. With reference to Figures 9 and 10, the maximum compressive stresses occur at the stagnation point, the circumferential stress being three and a half times as great as the meridional stress. The maximum tensile stresses occur in the vicinity of the maximum suction pressure as anticipated. The oscillatory nature of the stresses in the back portions of the shell probably is due to the nature of the approximate pressure distribution (Figure 4). The maximum combined stresses can be found in a straightforward fashion if desired. Figure 12 shows the stress resultants on the planes X = constant, that is, on sectors of the shell whose apex is the stagnation point and whose boundaries coincide with the approximate isobars considered (Figure 2). The contour $X = 0.91$ defines a circle which is tangent to the base circle, and, as indicated above, the stresses are not considered to be meaningful below the equatorial plane. The stresses on the section $X = 0.99$ are believed valid at all points; the situation is unclear for the intermediate section $X = 0.95$.

The components of displacement are shown in Figures 13, 14, and 15. A composition of displacements showing the deformed shape of the shell in

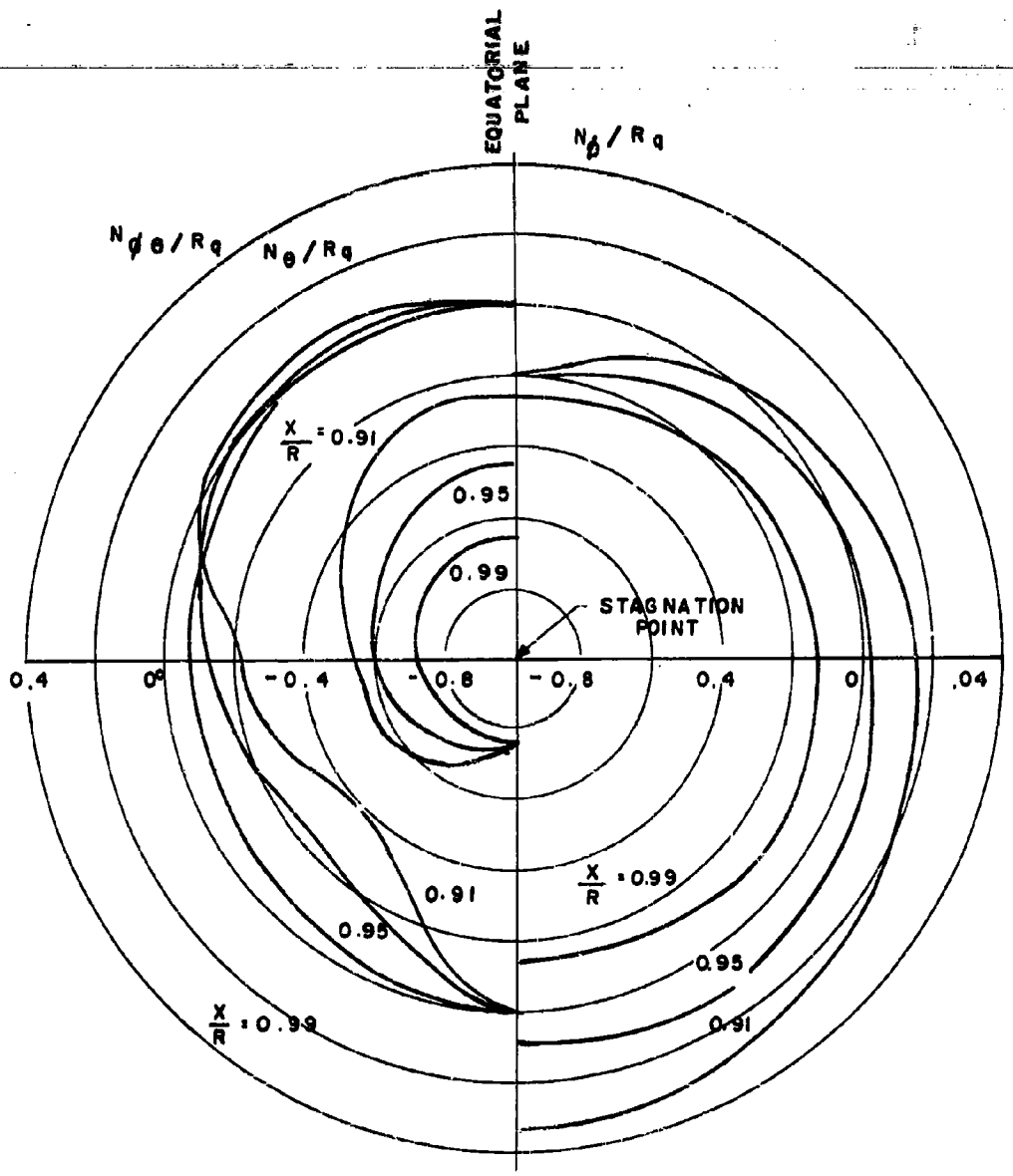

Figure 12. Stress Resultants on Circles X = constant

the planes $\theta = 0$ (vertical plane of symmetry containing the stagnation point) $\phi = \phi_0 = 115$ degrees (the base plane) and $\phi = 90$ degrees (the equatorial plane) are shown, respectively, in Figures 16, 17 and 18. The displacement pattern of Figure 17 suggests the nature of the edge moments and shears which must be applied to effect displacement constraint along the base circle.

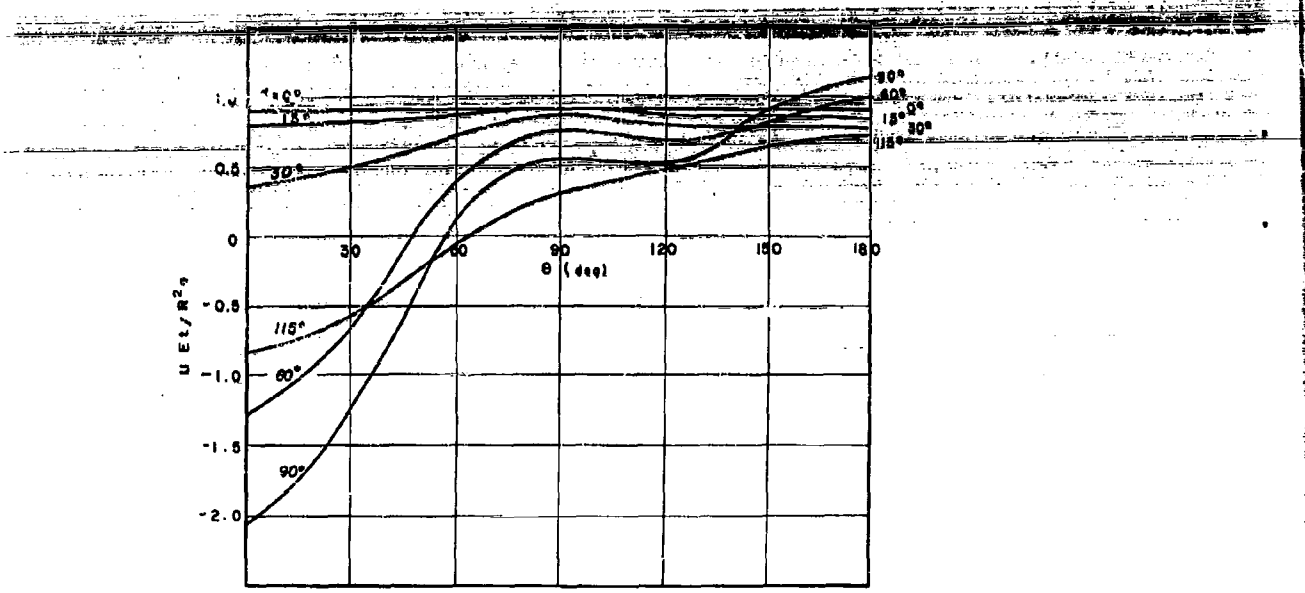

Figure 13. Radial Displacement u

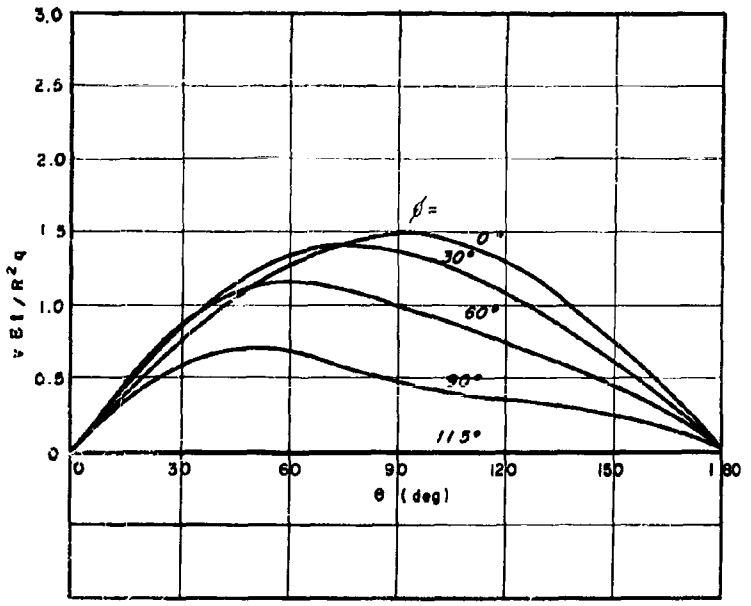

Figure 14. Circumferential Displacement v

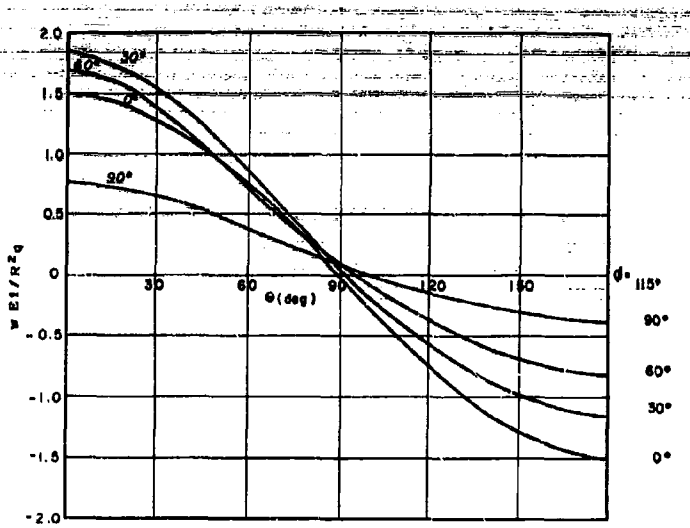

Figure 15. Meridional Displacement w

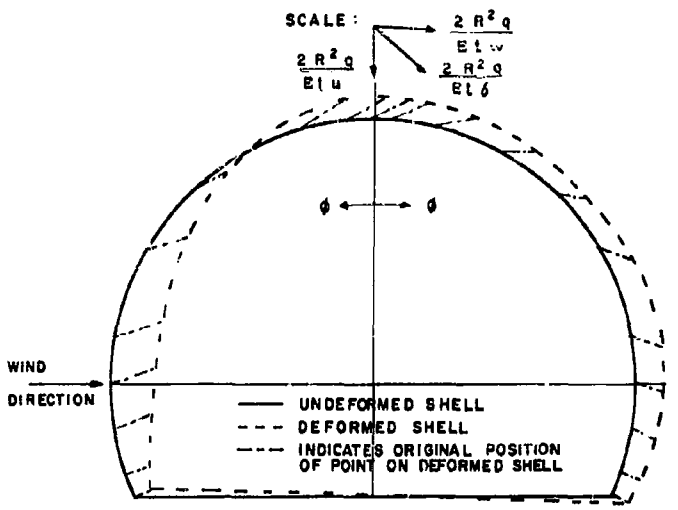

Figure 16. Deformed Shell in the Plane, $\theta = 0°, 180°$ (u, w displacements)

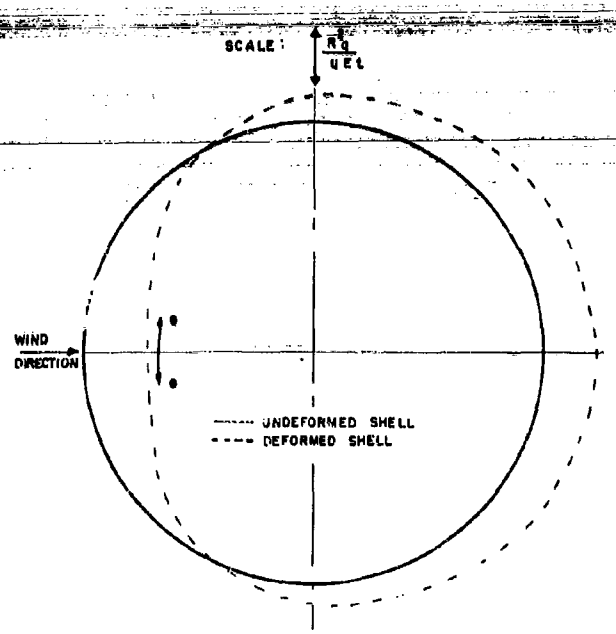

Figure 17. Deformed Shell in Base Circle Plane, $\phi = \phi_0 = 115°$ ($v = w = 0$, u displacements)

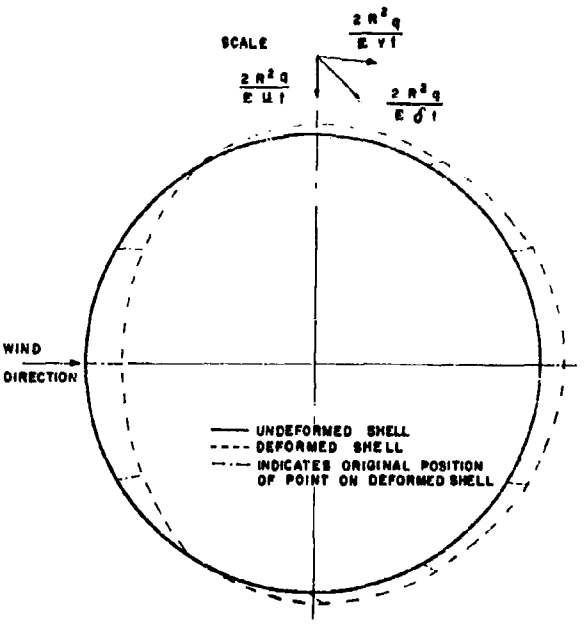

Figure 18. Deformed Shell in Equatorial Plane, $\phi = 90°$ (u, v displacements)

NOMENCLATURE FOR APPENDIX D

a_n, A_n	load parameters
$C_D = \frac{2D}{\pi R^2 q}$	drag coefficient
$C_L = \frac{L}{\pi R^2 q}$	lift coefficient
D	drag
E	Young's modulus of elasticity of shell material
$I_{1n}, I_{2n}, J_{1n}, J_{2n}$	integral expressions, Equations (42) and (47)
K_n, L_n, M_n	constants of integration
L	lift
N_θ	resultant circumferential force per unit length of shell cross section
N_ϕ	resultant meridional force per unit length of shell cross section
$N_{\theta\phi}$	resultant shearing force per unit length of shell cross section
P_n	pressure distribution parameter
p	pressure distribution normal to the undeformed shell surface
q	stagnation pressure
R	radius of shell
$S_{\phi n}$, $S_{\phi\theta n}$	meridional and shear stress components defined in Equation (39)
t	thickness of shell
u	radial displacement of shell
v	circumferential displacement of shell
w	meridional displacement of shell
X, $\overline{X}$	coordinates, see Figure 3
$\beta = \frac{R(1+\nu)}{E t}$	shell parameter
θ	meridional angle
ϕ	circumferential angle
Φ_0	angle of the base circle
ν	Poisson's ratio.

CATALOGUE FILE CARD

AD-

Rome Air Development Center.
Griffiss Air Force Base, New York.
GUIDE TO THE STRUCTURAL DESIGN OF TRUNCATED SPHERICAL RIGID GROUND RADOMES by Robert B. Curtis. June 1961. 48 pp. incl. illus. (Project No.: 5579; Task No.: 45384)(RADC-TR-61-84).

(Unclassified Report)

A compilation of the analytical operations for the structural analysis of a truncated spherical shell based jointly upon an evaluation of research effort and operational performance is presented. The four primary problem areas of loading, shell conversion, stability, and strength which confront the engineer in the structural design of such a shell are discussed in detail. In each of these problem areas, computational methods or approaches are offered which may be adopted as design procedure.

1. Radomes, Design of
2. Spherical Shell Design.
I. Curtis, Robert B.

AD-

Rome Air Development Center.
Griffiss Air Force Base, New York.
GUIDE TO THE STRUCTURAL DESIGN OF TRUNCATED SPHERICAL RIGID GROUND RADOMES by Robert B. Curtis. June 1961. 48 pp. incl. illus. (Project No.: 5579; Task No.: 45384)(RADC-TR-61-84).

(Unclassified Report)

A compilation of the analytical operations for the structural analysis of a truncated spherical shell based jointly upon an evaluation of research effort and operational performance is presented. The four primary problem areas of loading, shell conversion, stability, and strength which confront the engineer in the structural design of such a shell are discussed in detail. In each of these problem areas, computational methods or approaches are offered which may be adopted as design procedure.

1. Radomes, Design of
2. Spherical Shell Design.
I. Curtis, Robert B.

AD-

Rome Air Development Center.
Griffiss Air Force Base, New York.
GUIDE TO THE STRUCTURAL DESIGN OF TRUNCATED SPHERICAL RIGID GROUND RADOMES by Robert B. Curtis. June 1961. 48 pp. incl. illus. (Project No.: 5579; Task No.: 45384)(RADC-TR-61-84).

(Unclassified Report).

A compilation of the analytical operations for the structural analysis of a truncated spherical shell based jointly upon an evaluation of research effort and operational performance is presented. The four primary problem areas of loading, shell conversion, stability, and strength which confront the engineer in the structural design of such a shell are discussed in detail. In each of these problem areas, computational methods or approaches are offered which may be adopted as design procedure.

1. Radomes, Design of
2. Spherical Shell Design.
I. Curtis, Robert B.

AD-

Rome Air Development Center.
Griffiss Air Force Base, New York.
GUIDE TO THE STRUCTURAL DESIGN OF TRUNCATED SPHERICAL RIGID GROUND RADOMES by Robert B. Curtis. June 1961. 48 pp. incl. illus. (Project No.: 5579; Task No.: 45384)(RADC-TR-61-84).

(Unclassified Report)

A compilation of the analytical operations for the structural analysis of a truncated spherical shell based jointly upon an evaluation of research effort and operational performance is presented. The four primary problem areas of loading, shell conversion, stability, and strength which confront the engineer in the structural design of such a shell are discussed in detail. In each of these problem areas, computational methods or approaches are offered which may be adopted as design procedure.

1. Radomes, Design of
2. Spherical Shell Design.
I. Curtis, Robert B.